P H Y S I C A L   R E V I E W   L E T T E R S

Matter-Wave Bright Solitons in Spin-Orbit Coupled Bose-Einstein Condensates

V. Achilleos,[1] D. J. Frantzeskakis,[1] P. G. Kevrekidis,[2] and D. E. Pelinovsky[3]

[1]*Department of Physics, University of Athens, Panepistimiopolis, Zografos, Athens 15784, Greece*
[2]*Department of Mathematics and Statistics, University of Massachusetts, Amherst Massachusetts 01003-4515, USA*
[3]*Department of Mathematics, McMaster University, Hamilton, Ontario L8S 4K1, Canada*

We study matter-wave bright solitons in spin-orbit coupled Bose-Einstein condensates with attractive interactions. We use a multiscale expansion method to identify solution families for chemical potentials in the semi-infinite gap of the linear energy spectrum. Depending on the linear and spin-orbit coupling strengths, the solitons may present either a sech^2-shaped or a modulated density profile reminiscent of the stripe phase of spin-orbit coupled repulsive Bose-Einstein condensates. Our numerical results are in excellent agreement with our analytical findings and demonstrate the potential robustness of solitons for experimentally relevant conditions.

Introduction.—Gauge fields are ubiquitous in physics, as they are relevant to the interactions of charged particles with electromagnetic fields [1] or to fundamental interactions in elementary particle physics [2]. A variety of artificial gauge fields can be realized in ultracold atomic gases [3], as was also shown in recent experiments [4,5] with binary Bose-Einstein condensates (BECs). Importantly, synthetic magnetic fields can produce spin-orbit (SO) interactions in a BEC consisting of two hyperfine states of ^{87}Rb coupled by a Raman laser [5].

Different studies in SO coupled BECs have revealed the existence of a "stripe phase" [6] and phase transitions between that and other states [7]. Vortices with [8] or without [9] rotation, Skyrmions [10], Dirac monopoles [11], gray solitons [12], and self-trapped states (solitons) of an effective nonlinear Dirac equation [13], were also found. While the above studies refer to repulsive BECs, SO coupled BECs with *attractive interactions* have not been studied so far [14].

As it is known, attractive BECs can become themselves matter-wave bright solitons [15], i.e., self-trapped localized mesoscopic quantum systems with interesting applications [16]. Here, we demonstrate the existence, stability, and dynamics of matter-wave bright solitons in SO coupled attractive BECs, emerging in the semi-infinite gap of the linear spectrum. We find three distinct states having (a) zero momentum, (b) finite momentum, $+k_0$ or $-k_0$, and (c) stripe densities formed by the interference of the modes with $\pm k_0$ momentum; the spin polarization of all states is identified. We also show that branches (a) and (c) are generically stable, while branch (b) is stable for sufficiently small atom numbers. Hence, these solitons may be well within experimental reach.

Model.—We consider SO coupled BECs confined in a quasi-one-dimensional parabolic trap, with frequencies $\omega_x \ll \omega_\perp$. Assuming equal contributions of Rashba [17] and Dresselhaus [18] SO couplings (as in the experiment of

Ref. [5]), the mean-field energy functional of the system is $E = \int_{-\infty}^{+\infty} \mathcal{E} dx$, with

$$\mathcal{E} = \frac{1}{2}(\mathbf{\Psi}^\dagger \mathcal{H}_0 \mathbf{\Psi} + g_{11}|\psi_\uparrow|^4 + g_{22}|\psi_\downarrow|^4 + 2g_{12}|\psi_\uparrow|^2|\psi_\downarrow|^2), \tag{1}$$

where $\mathbf{\Psi} \equiv (\psi_\uparrow \psi_\downarrow)^T$, and the wave functions $\psi_\uparrow$ and $\psi_\downarrow$ are related to the two pseudospin components of the BEC. The single particle Hamiltonian $\mathcal{H}_0$ in Eq. (1) reads

$$\mathcal{H}_0 = \frac{1}{2m}(\hat{p}_x \mathbb{1} - k_L \hat{\sigma}_z)^2 + V_{\text{tr}}(x)\mathbb{1} + \Omega\hat{\sigma}_x, \tag{2}$$

where $\hat{p}_x = -i\hbar\partial_x$ is the momentum operator in the longitudinal direction, m is the atomic mass, $\hat{\sigma}_{x,z}$ are the Pauli matrices, $\mathbb{1}$ is the unit matrix, k_L is the wave number of the Raman laser which couples the two hyperfine states, $\Omega = \sqrt{2}\Omega_R$ is the Raman frequency, $V_{\text{tr}}(x) = m\omega_x^2 x^2/2$ is the parabolic trap, and the effective one-dimensional coupling constants, $g_{ij} = 2\alpha_{ij}\hbar\omega_\perp$ $(i, j = 1, 2)$, are defined by the s-wave scattering lengths α_{ij}; for attractive interactions, $\alpha_{ij} < 0$. Measuring the length in units of $a_\perp = \sqrt{\hbar/(m\omega_\perp)}$, time in units of $\omega_\perp^{-1}$, energy in units of $\hbar\omega_\perp$, and densities in units of $(2|\alpha_{11}|)^{-1}$, we derive from Eq. (1) dimensionless equations of motion for $\psi_{\uparrow,\downarrow}$:

$$i\partial_t\psi_\uparrow = \left(-\frac{1}{2}\partial_x^2 - ik_L\partial_x + V_{\text{tr}}(x) - |\psi_\uparrow|^2 - \beta|\psi_\downarrow|^2\right)\psi_\uparrow + \Omega\psi_\downarrow, \tag{3}$$

$$i\partial_t\psi_\downarrow = \left(-\frac{1}{2}\partial_x^2 + ik_L\partial_x + V_{\text{tr}}(x) - \beta|\psi_\uparrow|^2 - \gamma|\psi_\downarrow|^2\right)\psi_\downarrow + \Omega\psi_\uparrow, \tag{4}$$

where $V_{tr}(x) = (\omega_x/\omega_\perp)^2 x^2/2$, $\beta = |\alpha_{12}/\alpha_{11}|$, $\gamma = |\alpha_{22}/\alpha_{11}|$, and we have used $k_L \to k_L/a_\perp$ and $\Omega \to \Omega\hbar\omega_\perp$.

Variants of Eqs. (3) and (4) with $V_{tr} = 0$ have been studied in various contexts, ranging from field theory and the massive Thirring model [19] to nonlinear optics—in optical fiber gratings [20], birefringent optical fibers [21], and coupled optical wave guides [22]—and SO coupled repulsive BECs [13]. Solitons studied in these works were found to be stable only in nearly integrable cases [13,20,21]; in Ref. [22], so-called "embedded solitons" were generally found to be semistable. Here, we use a multiscale expansion method to derive approximate soliton solutions of Eqs. (3) and (4), which are stable for a wide range of experimentally relevant parameter values. Analytical results will be obtained for $\gamma = 1$ and $V_{tr} = 0$; the general case is investigated numerically.

Analytical results.—We start by seeking plane wave solutions of Eqs. (3) and (4), of the form $\psi_{\uparrow,\downarrow} = \psi_{1,2}\exp[i(kx - \omega t)]$, of constant amplitudes $\psi_{1,2} \ll 1$. Requiring that the resulting linearized, homogeneous system for $\psi_{1,2}$ has nontrivial solutions leads to the dispersion relation for the energy ω and momentum k,

$$\omega_\pm(k) = \frac{1}{2}k^2 \pm \sqrt{k_L^2 k^2 + \Omega^2}, \qquad (5)$$

which features two distinct branches–see Fig. 1. The upper branch $\omega_+(k)$ always has a minimum $(k, \omega) = (0, +\Omega)$, and the lower branch $\omega_-(k)$ has different behaviors depending on the sign of parameter $\Delta \equiv 1 - k_L^2/\Omega$: if $\Delta > 0$ then $\omega_-(k)$ has a minimum $(k, \omega) = (0, -\Omega)$ (region I); if $\Delta < 0$, $\omega_-(k)$ has a maximum $(k, \omega) = (0, -\Omega)$ and two minima $(\pm k_0, \omega_{min})$ (region II). Notice that the lowest energy states in region II may have either a positive or negative momentum $\pm k_0$ or they can be a linear superposition of both modes with momentum $\pm k_0$, thus forming the stripe phase [6].

As shown in Fig. 1, for energies $\omega < -\Omega$ in region I, or $\omega < \omega_{min}$ in region II, there exists a semi-infinite gap where linear modes do not propagate. However, matter-wave
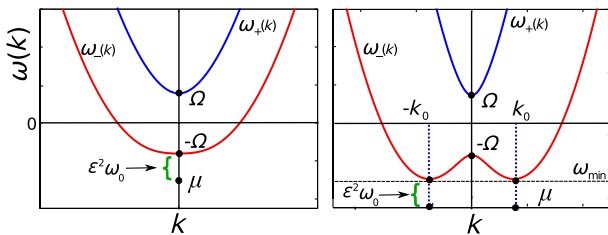

FIG. 1 (color online). Energy spectrum $\omega = \omega_\pm(k)$. The upper branch ω_+ (blue line) has a minimum $(k, \omega) = (0, \Omega)$ in both regions I (left panel) and II (right panel), for $k_L^2 < \Omega$ and $k_L^2 > \Omega$. The lower branch ω_- (red line) has a minimum (maximum) $(k, \omega) = (0, -\Omega)$ in region I (region II); in region II, there also exist two minima $(\pm k_0, \omega_{min})$.

bright solitons with energies inside the semi-infinite gap can be found analytically via a multiscale expansion method. Such solitons will have a chemical potential μ, defined as $\mu = -\Omega - \epsilon^2\omega_0$ in region I and $\mu = \omega_{min} - \epsilon^2\omega_0$ in region II; here, ϵ is a formal small parameter, and ω_0 is a free positive parameter [with $\omega_0/\Omega = \mathcal{O}(1)$], which sets the energy difference $\epsilon^2\omega_0$ from the linear limit inside the semi-infinite gap (see Fig. 1).

Accordingly, we seek solutions of Eqs. (3) and (4) in the form

$$\begin{pmatrix} \psi_\uparrow(x, t) \\ \psi_\downarrow(x, t) \end{pmatrix} = \begin{pmatrix} \epsilon A(X) \\ \epsilon B(X) \end{pmatrix} e^{i(Kx - \mu t)}, \qquad (6)$$

where $A(X)$ and $B(X)$ are unknown functions of the slow variable $X \equiv \epsilon x$, and momentum K is either $K = 0$ in region I or $K = \pm k_0$ in region II. Expanding $A(X)$ and $B(X)$ as series in ϵ, i.e., $A(X) = \sum_{n\geq 0}\epsilon^n a_n(X)$ and $B(X) = \sum_{n\geq 0}\epsilon^n b_n(X)$, and substituting the above expressions in Eqs. (3) and (4), we obtain the following.

In region I, the solvability conditions at the leading $[\mathcal{O}(\epsilon)]$ and first-order $[\mathcal{O}(\epsilon^2)]$ approximations are satisfied if $a_0 = -b_0 \equiv u(X)$ and $a_1 = b_1 = i(k_L/2\Omega)u'(X)$, where $u(X)$ is an unknown complex function (primes denote derivatives with respect to X). The latter is determined at the order $\mathcal{O}(\epsilon^3)$, where the solvability condition is the following stationary nonlinear Schrödinger equation:

$$u'' - \nu_1 u + \nu_2 |u|^2 u = 0, \qquad (7)$$

where the positive coefficients ν_1 and ν_2 are given by

$$\nu_1 = 2\omega_0\Delta^{-1}, \qquad \nu_2 = 2(1 + \beta)\Delta^{-1}.$$

In region II, for $K = \pm k_0$, the solvability condition at the leading order reads

$$a_0 = -\Omega^{-1}k_L(k_L \mp k_0)b_0 = u(X).$$

At the next order, we obtain a similar condition for a_1 and b_1:

$$k_L(k_L \pm k_0)a_1 + \Omega b_1 = i(k_L \pm k_0)u'(X).$$

Finally, at the order $\mathcal{O}(\epsilon^3)$, the solvability condition is again Eq. (7), but with coefficients ν_1 and ν_2 now given by

$$\nu_1 = \frac{2\omega_0 k_L^2}{k_0^2},$$

$$\nu_2 = \frac{2k_L(k_L \pm k_0)(k_L^4 + k_L^2 k_0^2 + \beta\Omega^2)}{\Omega^2 k_0^2}.$$

Taking into regard that the soliton solution of the stationary nonlinear Schrödinger equation, (7), is $u(X) = \sqrt{2\nu_1/\nu_2}\,\text{sech}(\sqrt{\nu_1}X)$, we end up with the approximate soliton solutions of Eqs. (3) and (4), characterized by the free parameter $\epsilon\sqrt{\omega_0}$. Solutions in region I read

$$\begin{pmatrix} \psi_\uparrow \\ \psi_\downarrow \end{pmatrix} \approx \epsilon \sqrt{\frac{2\omega_0}{1+\beta}} \mathrm{sech}\left(\epsilon\sqrt{\frac{2\omega_0}{\Delta}}x\right)\begin{pmatrix} 1 \\ -1 \end{pmatrix}e^{-i\mu t}, \quad (8)$$

where $\mu = -\Omega - \epsilon^2\omega_0$, while solutions in region II read

$$\begin{pmatrix} \psi_\uparrow \\ \psi_\downarrow \end{pmatrix} \approx \frac{\epsilon}{\sqrt{k_L \pm k_0}}f(x)\begin{pmatrix} \Omega \\ -k_L(k_L \pm k_0) \end{pmatrix}e^{\pm ik_0 x - i\mu t}, \quad (9)$$

where $\mu = \omega_{\min} - \epsilon^2\omega_0$ and the function $f(x)$ is given by

$$f(x) = \frac{\sqrt{2\omega_0 k_L}}{\sqrt{k_L^4 + k_L^2 k_0^2 + \beta\Omega^2}} \mathrm{sech}\left(\epsilon\sqrt{\frac{2\omega_0 k_L^2}{k_0^2}}x\right). \quad (10)$$

Equation (9) describes two different soliton solutions corresponding to $k = \pm k_0$. We can construct still another approximate soliton solution by using their linear combination. Particularly, Eqs. (3) and (4) for $\gamma = 1$ are compatible with the symmetry $\psi_\uparrow = -\bar{\psi}_\downarrow$ (the bar denotes complex conjugate) and the following solution satisfies this symmetry:

$$\begin{pmatrix} \psi_\uparrow \\ \psi_\downarrow \end{pmatrix} \approx \epsilon f(x)\begin{pmatrix} C_1 \cos(k_0 x) + iC_2\sin(k_0 x) \\ -C_1\cos(k_0 x) + iC_2\sin(k_0 x) \end{pmatrix}e^{-i\mu t},$$
$$(11)$$

where $\mu = \omega_{\min} - \epsilon^2\omega_0$, $C_1 = \Omega + k_L^2$, and $C_2 = -k_0 k_L$. Contrary to what is the case for the solutions of, Eqs. (8) and (9), which have a bell-shaped sech^2-density profile, the soliton (11) has a spatially modulated density profile (with a wavelength $2\pi/k_0$); thus, this "stripe soliton" (11) is analogous to the characteristic stripe phase of SO coupled repulsive BECs [6,7]. Note that only solutions (8) and (11) were considered in the numerical studies of Ref. [22]; solution (9), which does not satisfy the symmetry $\psi_\uparrow = -\bar{\psi}_\downarrow$, was not previously explored.

The above solutions describe different (normalized) longitudinal and transverse spin polarization of the solitons, given by $\tilde{\sigma}_{x,z} = \langle\sigma_{x,z}\rangle/(|\psi_\uparrow|^2 + |\psi_\downarrow|^2)$, where $\langle\sigma_{x,z}\rangle \equiv \mathbf{\Psi}^\dagger\hat{\sigma}_{x,z}\mathbf{\Psi}$: in region I, we find that the solitons are fully polarized along the x axis, i.e., $\tilde{\sigma}_x = -1$ (and $\tilde{\sigma}_z = 0$); in region II, the stripe soliton has again $\tilde{\sigma}_z = 0$, while the $\pm k_0$ soliton states are characterized by a finite $\tilde{\sigma}_z$, namely, $\tilde{\sigma}_z = \mp\sqrt{1 - (\Omega/k_0^2)^2}$ and $\tilde{\sigma}_x = -\Omega/k_0^2$. Thus, solitons' spin polarizations bear resemblance to those found for nonlinear states in SO coupled repulsive BECs [7].

Stability and numerical results.—In our numerical simulations, we have assumed a quasi-one-dimensional attractive BEC, confined in a trap with frequencies $\omega_x = 2\pi \times 20$ Hz and $\omega_\perp = 2\pi \times 1000$ Hz containing approximately 10^3 atoms, and scattering lengths ratios 1:0.8:1 (i.e., $\beta = 0.8$). We have fixed $\lambda_L \equiv 2\pi/k_L = 804$ nm, and varied the parameter Ω in the range $(1$–$10)E_L$, with $E_L = \hbar^2 k_L^2/2m$ (as in Ref. [5]), with m being the ^{7}Li mass. A fixed-point algorithm, and an initial ansatz pertaining to solutions (8)–(11) for regions I and II,
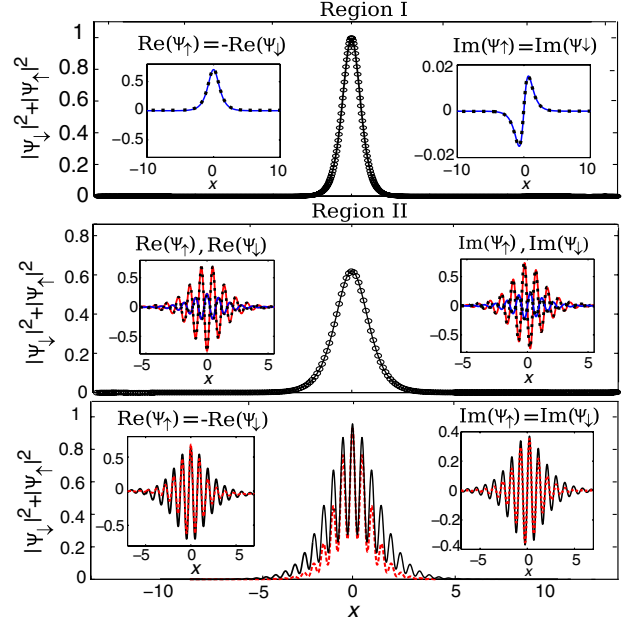

FIG. 2 (color online).   Density profiles of a bright soliton in region I (top), a $+k_0$ soliton (middle), and a stripe soliton (bottom) in region II. Solid line and circles (or dashed lines) depict, respectively, the analytical results of Eqs. (8)–(11), and the numerically found solutions. Left and right insets show, respectively, the real and imaginary parts of $\psi_\uparrow$ (blue) and $\psi_\downarrow$ (red). Parameters are $\Omega = 120$ and $\epsilon^2\omega_0 = 0.4$ (region I), or $\Omega = 35$ and $\epsilon^2\omega_0 = 0.4$ (region II); in both regions $k_L = 8$ and $\beta = 0.8$.

was used to find respective numerical solutions, which are exact ones (up to a prescribed numerical tolerance). Examples, for both regions I and II, are provided in Fig. 2, where the density profiles, $|\psi_\uparrow|^2 + |\psi_\downarrow|^2$, as well as the real and imaginary parts (insets) are shown. It is observed that solitons in region I and stripe solitons in region II respect the symmetry $\psi_\uparrow = -\bar{\psi}_\downarrow$, while the k_0 soliton in region II does not. The approximate analytical results (solid lines) are in excellent agreement with the full numerical ones (circles and dashed lines). Furthermore, we have confirmed the existence of the soliton families for $\gamma \neq 1$ in a relatively wide range of values, i.e., for $0.5 \leq \gamma \leq 1.5$.

We have also studied the stability of the solitons. Since the energies of solitons lie inside the semi-infinite gap, their spectral stability is controlled by the negative index count (see Chap. 4 of Ref. [23]). We write the spectral stability problem as

$$H\mathbf{u} = i\lambda J\mathbf{u}, \quad (12)$$

where $\mathbf{u}$ is a 4×1 vector of the perturbations to $[\psi_\uparrow, \bar{\psi}_\uparrow, \psi_\downarrow, \bar{\psi}_\downarrow]$, H is a 4×4 self-adjoint matrix operator associated with the right-hand side of Eqs. (3) and (4) linearized around the solitons, $J = \mathrm{diag}(1, -1, 1, -1)$, and λ is a spectral parameter with the instability growth rate given
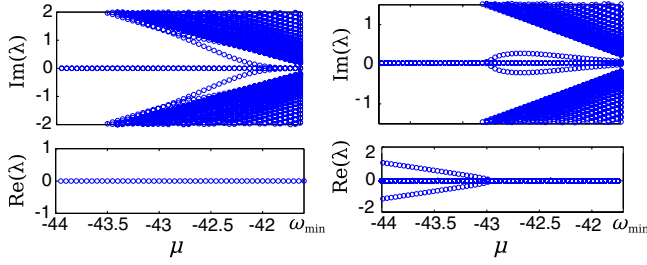
FIG. 3 (color online). Eigenvalues obtained from the spectral problem, Eq. (12), for the stripe soliton (left) and $+k_0$-soliton (right) branches. The latter becomes spectrally unstable due to the eigenvalue pair with $\text{Re}(\lambda) \neq 0$ for $\mu \lesssim -42.9$. Parameters are as in Fig. 2.
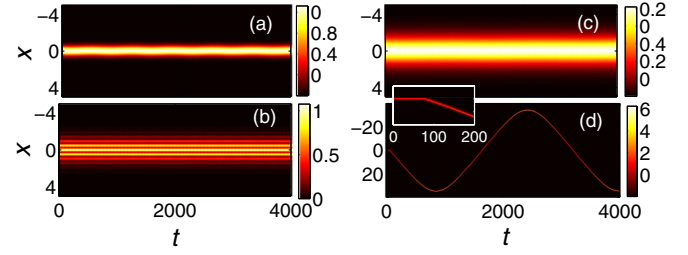

FIG. 4 (color online). Contour plots showing the evolution of the total density for solitons in region I (a) and region II (b)–(d). Panel (b): Stripe soliton; panels (c) and (d): $+k_0$ solitons with $\mu = -41.77 > \mu_c$ and $\mu = -43 < \mu_c$. Other parameters are as in Fig. 2 (but with $\Omega = 70$ for region I) but now for $\gamma = 0.8$ and $\omega_x/\omega_z = 0.02$.

by $\text{Re}(\lambda)$ (if positive). The operator H has a finite number of negative eigenvalues, denoted by $n(H)$, and a two-dimensional kernel spanned by the symmetries of Eqs. (3) and (4) :

$$\mathbf{u}_1 = [i\psi_\uparrow, -i\bar{\psi}_\uparrow, i\psi_\downarrow, -i\bar{\psi}_\downarrow],$$
$$\mathbf{u}_2 = \partial_x[\psi_\uparrow, \bar{\psi}_\uparrow, \psi_\downarrow, \bar{\psi}_\downarrow].$$

Associated with the eigenvectors of H, there exist generalized eigenvectors of the spectral stability problem, Eq. (12), given by solutions of the inhomogeneous equations

$$H\mathbf{v}_j = iJ\mathbf{u}_j, \qquad j = 1, 2. \qquad (13)$$

Computing the symmetric matrix of symplectic projections with elements $D_{lj} = \langle \mathbf{v}_l, iJ\mathbf{u}_j \rangle$ ($l, j = 1, 2$), where $\langle \cdot, \cdot \rangle$ is a standard inner product, we denote the number of negative eigenvalues of D by $n(D)$. The negative index count is now given by # $= n(H) - n(D)$ and this number determines the number of unstable eigenvalues with $\text{Re}(\lambda) > 0$ and/or the number of potentially unstable eigenvalues with $\text{Re}(\lambda) = 0$ and negative energy in the spectral stability problem, Eq. (12) [23].

To assess the stability of solitons in regions I and II, we have computed indices $n(H)$ and $n(D)$ by numerically solving the eigenvalue problem (12) and Eq. (13) (this was done by using a 2nd-order difference scheme and an Arnoldi-type method). For solitons in region I and the stripe solitons in region II, we have found that $n(H) = 1$ and $n(D) = 1$ in their existence intervals; therefore, the negative index # is zero. This ensures spectral stability of these solitons. On the other hand, for $\pm k_0$ solitons in region II, $n(H) = 3$ in the existence interval, but $n(D)$ changes from 1 near the bifurcation at $\mu = \omega_{\min}$ to 2 for smaller values of μ. Therefore, the negative index is # $= 2$ near the bifurcation at $\mu = \omega_{\min}$, due to a pair of negative energy yet neutrally stable eigenvalues in the spectrum of Eq. (12). For smaller values of μ, it switches to # $= 1$ indicating a real unstable eigenvalue.

Figure 3 illustrates the above behavior by depicting the dependence of the eigenvalues λ on μ, for the stripe and k_0 solitons in region II. The spectrum of the stripe soliton

(left panel) consists of purely imaginary eigenvalues, indicating spectral stability; note that a pair of eigenvalues departs from $\mu \approx \omega_{\min}$ and grows, but eventually collides with the rest of the spectrum for decreasing μ, without inducing any instability. On the other hand, the spectrum of the $+k_0$ soliton (right panel) indicates the emergence of an instability when a pair of neutrally stable eigenvalues of negative energy crosses zero at $\mu = \mu_c \approx -42.9$ and splits along the real axis for smaller μ, yielding an exponential growth of perturbations. This zero crossing occurs when the negative index count # changes from 2 to 1.

Numerical soliton solutions were also obtained for $\gamma \neq 1$ and $V_{\text{tr}} \neq 0$ and their dynamics was investigated. These solutions were perturbed by a noise of strength $\approx 10\%$ of their initial amplitudes, and used as initial conditions for Eqs. (3) and (4), which were then numerically integrated via a 4th-order Runge-Kutta method. As shown in Fig. 4, solitons in region I [panel (a)], stripe solitons in region II [panel (b)], and k_0 solitons with $\mu = -41.77 > \mu_c$, corresponding to their stability region [panel (c)], are robust up to $t = 4000$ (≈ 1 sec), which was the time of the simulation. An example of unstable k_0 solitons with $\mu = -43 < \mu_c$ is also illustrated [panel (d)]: the soliton departs from an unstable position for short times [see inset in panel (d)] but later is reflected due to the trap and oscillates therein. Note in the absence of the trap, the dynamics are as in Fig. 4, but with the difference that, after the onset of the instability, the unstable k_0 soliton moves steadily with a nearly constant speed [cf. inset in panel (d) of Fig. 4].

We stress that although our analytical results were obtained in the cases $\gamma = 1$ and $V_{\text{tr}} = 0$, the simulations have revealed the existence and stability of solitons for a wide range of values $\gamma \neq 1$ in the presence of the trap and for different values of β. This clearly indicates that the presented matter-wave soliton families have an excellent chance to be observed in experiments with SO coupled attractive BECs.

Conclusions.—In summary, we have used a multiscale expansion method to identify matter-wave bright soliton

states in SO coupled attractive BECs. The solitons, characterized by a chemical potential residing in the semi-infinite gap of the linear spectrum, were approximated analytically and shown to exhibit either a sech^2-shaped or a modulated density profile, strongly reminiscent of the stripe phase of SO coupled repulsive BECs. Our analytical predictions were corroborated by numerical simulations, which have shown that the solitons exist and are generally robust for a wide range of the physical parameters involved even in the presence of noise. An interesting future direction is the investigation of higher-dimensional generalizations and collapse [24] for the solitons presented above. One can then explore (as in Ref. [25]) time- or space-dependent potentials, nonlinearities, and gain or loss, and identify robust three-dimensional solitons.

[1] J. J. Sakurai, *Modern Quantum Mechanics* (Addison-Wesley, Reading, MA, 1994).

[2] M. E. Peskin and D. V. Schroeder, *An Introduction to Quantum Field Theory* (Westview Press, Boulder, 1995).

[3] J. Dalibard, F. Gerbier, G. Juzeliūnas, and P. Öhberg, Rev. Mod. Phys. **83,** 1523 (2011).

[4] Y.-J. Lin, R. L. Compton, K. Jimenez-Garcia, J. V. Porto, and I. B. Spielman, Nature (London) **462,** 628 (2009).

[5] Y.-J. Lin, K. Jimenez-Garcia, and I. B. Spielman, Nature (London) **471,** 83 (2011).

[6] T. L. Ho and S. Zhang, Phys. Rev. Lett. **107,** 150403 (2011); S. Sinha, R. Nath, and L. Santos, Phys. Rev. Lett. **107,** 270401 (2011).

[7] Y. Li, L. P. Pitaevskii, and S. Stringari, Phys. Rev. Lett. **108,** 225301 (2012).

[8] X.-Q. Xu and J. H. Han, Phys. Rev. Lett. **107,** 200401 (2011).

[9] J. Radić, T. A. Sedrakyan, I. B. Spielman, and V. Galitski, Phys. Rev. A **84,** 063604 (2011); B. Ramachandhran, B. Opanchuk, X-J. Liu, H Pu, P. D. Drummond, and H. Hu, Phys. Rev. A **85,** 023606 (2012).

[10] T. Kawakami, T. Mizushima, M. Nitta, and K. Machida, Phys. Rev. Lett. **109,** 015301 (2012).

[11] G. J. Conduit, Phys. Rev. A **86,** 021605(R) (2012).

[12] O. Fialko, J. Brand, and U. Zülicke, Phys. Rev. A **85,** 051605(R) (2012).

[13] M. Merkl, A. Jacob, F. E. Zimmer, P. Öhberg, and L. Santos, Phys. Rev. Lett. **104,** 073603 (2010).

[14] After the preprint of this work was posted (arXiv:1211.0199), an additional study on this theme appeared, which was later published as Y. Xu, Y. Zhang, and B. Wu, Phys. Rev. A **87,** 013614 (2013).

[15] K. E. Strecker, G. B. Partridge, A. G. Truscott, and R. G. Hulet, Nature (London) **417,** 150 (2002); L. Khaykovich, F. Schreck, G. Ferrari, T. Bourdel, J. Cubizolles, L. D. Carr, Y. Castin, C. Salomon, Science **296,** 1290 (2002); S. L. Cornish, S. T. Thompson, and C. E. Wieman, Phys. Rev. Lett. **96,** 170401 (2006).

[16] T. Billam, A. L. Marchant, S. L. Cornish, S. A. Gardiner, and N. G. Parker, in *Spontaneous Symmetry Breaking, Self-Trapping, and Josephson Oscillations* edited by, B. A. Malomed (Springer-Verlag, Berlin, 2013), pp. 403–455.

[17] Y. A. Bychkov and E. I. Rashba, J. Phys. C **17,** 6039 (1984).

[18] G. Dresselhaus, Phys. Rev. **100,** 580 (1955).

[19] W. E. Thirring, Ann. Phys. (N.Y.) **3,** 91 (1958).

[20] D. N. Christodoulides and R. I. Joseph, Phys. Rev. Lett. **62,** 1746 (1989); A. Aceves and S. Wabnitz, Phys. Lett. A **141,** 37 (1989).

[21] B. A. Malomed, Phys. Rev. A **43,** 410 (1991).

[22] A. R. Champneys, B. A. Malomed, and M. J. Friedman, Phys. Rev. Lett. **80,** 4169 (1998).

[23] D. E. Pelinovsky, *Localization in Periodic Potentials: From Schrödinger Operators to the Gross–Pitaevskii Equation* (Cambridge University Press, Cambridge, 2011).

[24] C. Sulem and P. L. Sulem, *The Nonlinear Schrödinger Equation* (Springer-Verlag, New York, 1999).

[25] Z. Yan and C. Hang, Phys. Rev. A **80,** 063626 (2009); Z. Yan and V. V. Konotop, Phys. Rev. E **80,** 036607 (2009).